Cellular/Molecular

Visualization of Glucocorticoid Receptor and Mineralocorticoid Receptor Interactions in Living Cells with GFP-Based Fluorescence Resonance Energy Transfer

Mayumi Nishi, Masayuki Tanaka, Ken-ichi Matsuda, Masataka Sunaguchi, and Mitsuhiro Kawata
Department of Anatomy and Neurobiology, Kyoto Prefectural University of Medicine, Kyoto 602-8566, Japan

Adrenal corticosteroids readily enter the brain and exert markedly diverse effects, including stress responses in the target neural cells via two receptor systems, the mineralocorticoid receptor (MR) and the glucocorticoid receptor (GR). It has been shown that the GR and MR are highly colocalized in the hippocampus. Given the differential action of the MR and GR in the hippocampal region, it is important to elucidate how these receptors interact with each other in response to corticosteroids. We investigated the heterodimerization of the MR and GR with green fluorescent protein-based fluorescence resonance energy transfer (FRET) microscopy in living cells with spatiotemporal manner. FRET was evaluated in three ways: (1) ratio imaging; (2) emission spectra; and (3) acceptor photobleaching. FRET analysis demonstrated that cyan fluorescent protein–GR and yellow fluorescent protein–MR form heterodimers after corticosterone (CORT) treatment both in the nucleus of cultured hippocampal neurons and COS-1 cells, whereas they do not form heterodimers in the cytoplasm. The content of the GR–MR heterodimer was higher at 10^{-6} M CORT than at 10^{-9} M CORT and reached a maximum level after 60 min of CORT treatment in both cultured hippocampal neurons and COS-1 cells. The distribution pattern of heterodimers in the nucleus of cultured hippocampal neurons was more restricted than that in COS-1 cells. The present study using mutant fusion proteins in nuclear localization signal showed that these corticosteroid receptors are not translocated into the nucleus in the form of heterodimers even after treatment with ligand and thus allow no heterodimerization to take place in the cytoplasm. These results obtained with FRET analyses give new insights into the sites, time course, and effects of ligand concentration on heterodimersization of the GR and MR.

Key words: **corticosteroid receptor; heterodimer; FRET; hippocampus; stress; GFP**

Introduction

Adrenal corticosteroids [cortisol in humans or corticosterone (CORT) in rodents] exert numerous effects in the CNS that regulate stress response, mood, learning and memory, and various neuroendocrine functions (McEwen et al., 1986; de Kloet, 1991; McEwen, 1991). CORT actions in the brain are mediated by the glucocorticoid receptor (GR) and mineralocorticoid receptor (MR), both of which are ligand-inducible transcriptional factors. The GR and MR show a high degree of colocalization in the hippocampus (Arriza et al., 1988; de Kloet et al., 1998). Because the MR has ~10-fold higher affinity for CORT than the GR, hippocampal MR responds strongly to CORT (Krozowski and Funder, 1983; Beaumont and Fanestil, 1988; Rupprecht et al., 1993). Thus, in the hippocampus, this one compound, CORT, serves to regulate the two signaling pathways via the MR and GR (Reul and de Kloet, 1985; Pearce and Yamamoto, 1993; Kawata, 1995). The progressive activation of the MR at a low CORT concentration and additional activation of the GR when CORT levels increase can cause extreme alterations of neuronal integrity for responding to stress conditions (Magarinos et al., 1996; Gould et al., 1997) and neuronal functions, such as changes in neuronal excitability (Joels and de Kloet 1992), associated with changes in neuroendocrine regulation and behavior.

In studying these processes, the subcellular dynamics of both receptors are one of the most important issues. Several investigations have followed subcellular trafficking of MR and GR in living cells using green fluorescent protein (GFP) and its color variants (Htun et al., 1996; Fejes-Toth et al., 1998; Nishi et al., 2001; DeFranco, 2002). Furthermore, McNally et al. (2000) showed that the hormone-occupied GR undergoes a rapid exchange between chromatin and the nucleoplasmic compartment by using the fluorescent recovery after photobleaching technique (Reits and Neefjes, 2001). We focused on the spatiotemporal-specific interactions between GR and MR in living cells. It has been demonstrated that these receptors bind as homodimers to the same hormone response elements (HREs) (Umesono and Evans, 1989). However, physiological studies in various systems suggest that the GR and MR also functionally interact with each other (Gomez-Sanchez et al., 1990; Joels and de Kloet, 1992, 1994). Previous investigators reported that GR–MR heterodimerization takes place and indicated that functional interactions between

Received Dec. 14, 2003; revised April 5, 2004; accepted April 9, 2004.

This work was supported in part by Grants-in-Aid for Scientific Research from the Ministry of Education, Culture, Sports, Science, and Technology to M.N. and M.K. We thank Dr. Satoshi Kida for providing plasmids of CFP–YFP. We are grateful to Dr. Yasunori Hayashi for valuable discussions.

Correspondence should be addressed to Dr. Mayumi Nishi, Department of Anatomy and Neurobiology, Kyoto Prefectural University of Medicine, Kawaramachi Hirokoji, Kamigyo-ku, Kyoto 602-8566, Japan. E-mail: nmayumi@koto.kpu-m.ac.jp.

DOI:10.1523/JNEUROSCI.5495-03.2004

 0270-6474/04/244918-10$15.00/0

GR and MR using reporter assay (Trapp et al., 1994; Liu et al., 1995; Savory et al., 2001). But these studies examined heterodimerization only in whole-cell extracts, not in a spatiotemporal-specific manner maintaining intact cell structures. We, therefore, looked for heterodimerization of GR and MR in living cells by using GFP-based fluorescence resonance energy transfer (FRET) microscopy. Our findings indicated that the GR and MR can form heterodimers in the nucleus after ligand treatment. Cotransfection studies of cyan fluorescent protein (CFP)–GR mutant containing mutations in the domain of nuclear localization signal 1 (Savory et al., 1999) and wild-type yellow fluorescent protein (YFP)–MR have shown that the receptors do not form a heterodimer in the cytoplasm even after ligand treatment.

Here, we report for the first time the dynamic interaction between GR and MR in a spatiotemporal-specific manner using the FRET technique in living cultured hippocampal neurons and non-neural cells.

Materials and Methods

Plasmid construct

The **6RMR** vector (provided by Dr. S. J. Watson, Mental Health Research Institute, University of Michigan Medical School, Ann Arbor, MI) containing the rat hippocampus MR cDNA was digested with *Sal*I. The MR cDNA obtained was ligated in frame into the *Xho*I site in the multiple cloning site of **pEGFPC1** or **pEYFPC1** (Clontech, Palo Alto, CA) using a ligation kit (Takara, Kusatsu, Japan). The **6RGR** vector (provided by Dr. K. R. Yamamoto, Department Biochemistry and Biophysics, University of California, San Francisco, CA) containing the rat liver GR cDNA was digested at the *Bam*HI sites and subcloned into the **pGEM-4** vector (Promega, Madison, WI), resulting in **pGEM-4-GR**. The GR cDNA with a truncated 5′ coding region was isolated from **pGEM-4-GR** by *EaeI-Bam*HI digestion and ligated in frame into the multiple cloning site (*Bsp120I and Bam*HI) of **pEGFPC1** or **pECFPC1** (Clontech) using a ligation kit (Takara). The mutant of CFP–GR deficient in NL1 function of GR (CFP–GRNL1$^-$) was created by mutating amino acids ^{513}KKK^{515} of wild-type rat GR to ^{513}NNN^{515} by site-directed mutagenesis according to a previous study (Savory et al., 2001). The mutagenesis of NL1 of GR was performed by using the QuickChange Site-Directed Mutagenesis kit (Stratagene, La Jolla, CA) according to the manufacturer's instructions, and these mutations were confirmed by DNA sequencing. The **pUC-ER6** vector (provided by Dr. M. Muramatsu, Department of Biochemistry, Saitama Medical School, Saitama, Japan) containing rat estrogen receptor α (ERα) cDNA was introduced with *Xho*I site just upstream of the first ATG using the QuickChange Site-Directed Mutagenesis kit (Stratagene). After cutting with *Xho*I and *Eco*RI, the gene was subcloned into **pEGFPC1** or **pEYFPC1** vector. Positive control for a FRET experiment, a CFP–YFP construct was used in which CFP and YFP were tandemly linked via three glycine residues.

Cell culture and transfection

Dissociated hippocampal primary neuronal cultures were prepared from 18-d-old Sprague Dawley rat fetuses according to a previously reported method (Nishi et al., 1999). Briefly, the rat fetuses were removed from the placenta in a laminar flow hood and transferred to ice-cold dissecting solution (0.8% NaCl, 0.04% KCl, 0.006% Na_2HPO_4.12H2O, 0.003% KH_2PO_4, 0.5% glucose, 0.00012% phenol red, 0.0125% penicillin G, and 0.02% streptomycin). The isolated hippocampus was mechanically dissociated by triturating through a fire-polished glass pipette. The dissociated cells were plated on a 35 mm glass-bottomed dish precoated with 0.1 mg/ml polyethylenimine (Sigma, St. Louis, MO) at an initial plating density of 1×10^5 cells/well by adding 200 μl of the cell suspension to each well (glass-bottomed area of 0.78 cm^2; Matsunami Glass, Tokyo, Japan). The cultures were maintained in complete neuronal medium (CNM) consisting of 92.5% (v/v) Eagle's MEM (Sigma), 1% (w/v) nonessential amino acids (Invitrogen, Gaithersburg, MD), 0.16% (w/v) glucose, and 5% (v/v) FCS (Sigma) in a CO_2 incubator at 37°C with 5% CO_2/95% air. COS-1 cells were maintained in DMEM (Sigma), without phenol red, supplemented with 10% FCS overnight in a 4-well multidish with 16 mm diameter (Nunc, Roskilde, Denmark) at an initial plating density of 2×10^4 cells/well in 400 μl of medium.

Plasmid DNA was transiently transfected into cells by a liposome-mediated method using LipofectAMINE PLUS (Invitrogen) according to the manufacturer's instructions. Hippocampal neuronal cells were cultured in CNM for 48 hr and then treated with 1 mM cytosine-b-D-arabinofuranoside for 24 hr to suppress the proliferation of glial cells. Hippocampal neuronal cells were cultured in serum-free medium (SFM) without steroids (MEM with 0.16% of glucose, 1% nonessential amino acids, 20 mM putrescine, 15 nM sodium selenite, 5 μg/ml insulin, and 100 μg/ml transferrin) for 48 hr before transfection. For COS-1 cells, the medium was replaced with SFM 2 hr before transfection. Cells were transfected with 200 μl of OPTI MEM (Invitrogen) containing 8 μl of LipofectAMINE solution and 200 ng of plasmid DNA per well of 1×10^5 cells for 5 hr at 37°C. For ligand stimulation, cells were washed in SFM and treated with 10^{-6} or 10^{-9} M CORT (Sigma). As a negative control, cells were treated with 10^{-8} M 17β-Estradiol.

Immunoprecipitation

COS-1 cells cotransfected with YFP–MR and CFP–GR were scraped with ice-cold lysis buffer [50 mM Tris, 500 mM NaCl, 2 mM EDTA, 1% NP-40, 0.5% Triton-X, and Complete proteinase inhibitor mixture (Nakalai, Japan), pH 7.5] and centrifuged at 15,000 rpm for 15 min at 4°C. The supernatant was preincubated with pre-cleaned protein G-Sepharose (Pharmacia Biotech, Peapack, NJ). After centrifugation, the supernatant was incubated with anti-MR antibody (Ito et al., 2000) for 1 hr at 4°C and then protein G-Sepharose for 1 hr at 4°C with rocking. After washing the beads three times with lysis buffer, immunoprecipitated proteins were boiled for 5 min in SDS-PAGE sample buffer and subjected to immunoblotting analysis as described previously (Nishi et al., 1999). Briefly, proteins were separated by a 7.5% SDS-PAGE, and samples were electroblotted on polyvinylidene difluoride membranes (Immobilon-P; Millipore, Bedford, MA) by using a semi-dry blotting apparatus (Transblot-SD; Bio-Rad, Hercules, CA). The membranes were incubated with anti-GR (1:5000 dilution) (Morimoto et al., 1996) overnight at 4°C. Secondary goat anti-rabbit–HRP (Bio-Rad) was added at a 1:5000 dilution for 1 hr at room temperature. Blots were visualized using ECL (Amersham, Buckinghamshire, UK).

Time-lapse image acquisition and analysis

For the living cell imaging experiments, the culture medium was replaced with SFM buffered with 20 mM HEPES (Sigma), and the image acquisition was performed in a temperature-controlled room at 37°C. Images were acquired using a Quantix high-resolution, cooled CCD camera (Photometrics, Tucson, AZ) attached to a microscope (IXL70; Olympus, Tokyo, Japan) equipped with an epifluorescence attachment. For the observation of neurons, a 60× objective lens was used, whereas COS-1 cells were observed with a 40× objective lens. GFP fluorescence was observed with a 480 nm excitation filter, 515 nm emission filter, and a 505 nm dichroic mirror (Olympus); YFP fluorescence with a 500AF25 nm excitation filter, a 545AF35 nm emission filter, and a 525DRLP dichroic mirror (Omega Optical, Brattleboro, VT); and CFP fluorescence with a 440AF21 nm excitation filter, a 480AF30 nm emission filter, and a 455DRLP dichroic mirror (Omega Optical). Data were evaluated with image analysis software, MetaMorph and MetaFlour (Universal Imaging West Chester, PA). Confocal scanning laser microscopic images were collected with an LSM 510 confocal microscope (Zeiss, Jena, Germany) equipped with an argon ion laser, a helium–neon laser, and a ×63 oil immersion objective lens (numerical aperture, 1.4; Zeiss).

FRET analysis

Protein–protein interactions of CFP–GR and YFP–MR were studied using FRET microscopy in COS-1 cells and cultured hippocampal neurons. FRET was evaluated in three ways: (1) ratio imaging; (2) emission spectra by the Emission Fingerprinting method using LSM 510 META (Zeiss); and (3) acceptor photobleaching. In all FRET experiments, cells showing nearly the same fluorescence intensity of donor and acceptor were selected for analysis.

Ratio imaging. For ratio imaging FRET microscopy, images were taken

with the donor filter set for CFP as described above and with a FRET filter set (XF88; Omega Optical), which consisted of a 440AF21 excitation filter for the donor, a 455DRPL dichroic mirror, and a 535AF26 emission filter for the acceptor. Images were captured with both filter sets under identical conditions, and ratio images were calculated by dividing FRET (acceptor–filter image) by CFP (donor image) using MetaMorph software according to the manufacturer's instructions after appropriate background subtraction (i.e., background fluorescence was measured in a space in which no cell was present, and total fluorescence was then subtracted from background fluorescence) (Tanaka et al., 2003). Ratio images were pseudocolored, in which the red range indicated a high ratio and the blue range indicated a low ratio. To prevent the detection of false positive FRET images, the imaging conditions were adjusted to favor donor emission over acceptor emission. We have confirmed that the level of bleed-through of CFP and YFP in our filter sets was very low (Tanaka et al., 2003). The data shown are representative images obtained from three independent experiments.

Emission spectra. For detecting emission spectral changes in FRET imaging, the Emission Fingerprinting method using confocal laser-scanning microscope LSM 510 META (Zeiss) was used. First, spectral signatures of the fluorescence within the specimen were captured by means of lambda stack acquisition with excitation at 458 nm and detection at 10 nm intervals from 458 through 596 nm using an HFT 458/543 dichroic mirror. Several regions of interest (ROI) with a diameter of 2 μm were then randomly selected for obtaining emission spectral patterns, and the mean ratio of fluorescence intensity of 527 nm and 474 nm was calculated from selected ROI at each time point after ligand addition (20 ROI per cell in 10 cells from three independent experiments). Because the levels of protein expression in each cell were not exactly the same, especially between donor and acceptor molecules, we normalized the fluorescence intensity in each cell by dividing the mean ratio of fluorescence intensity after ligand treatment by that before ligand treatment.

Acceptor photobleaching. For acceptor photobleaching, we used the confocal laser-scanning microscope (Kinoshita et al., 2001). Energy transfer was detected as an increase in donor fluorescence (CFP) after photobleaching of the acceptor molecules (YFP). The acceptor was photobleached by using a 514 nm laser for 1 min at maximum power (25 mW) after 60 and 90 min of 10^{-6} and 10^{-9} M CORT treatment, respectively. The cells were then subjected to emission spectral analysis as described above for detecting the changes in fluorescence intensity of the donor molecule. The increase in donor fluorescence intensity was shown as a percentage. We analyzed 10 cells from three independent experiments.

Statistics

All results are expressed as means ± SEM values. The significance of differences between the mean of various groups was determined by Student's *t* test for independent samples.

Results

Properties of fusion proteins

The mutants of CFP–GRNL1$^-$, wild-type CFP–GR, YFP–MRNL$^-$, and wild-type YFP–MR were transiently transfected to COS-1 cells and analyzed by immunoblotting. Fusion proteins of CFP–GRNL1$^-$ showed the expected molecular mass of 110 kDa, the same molecular mass as that of the wild-type protein, when transiently transfected into COS-1 cells (Fig. 1*A*). We thus confirmed that the DNA sequences of mutation sites in chimera construct were correct.

We have shown previously that GFP–GR (Nishi et al., 1999), GFP–MR, CFP–GR, YFP–MR (Nishi et al., 2001), CFP–ERα, and YFP–ERα (Matsuda et al., 2002) fusion proteins retained their normal expression patterns, expected molecular masses, and functional abilities when transiently transfected into COS-1 cells.

Immunoprecipitation

To look for heterodimerization of the GR and MR, we analyzed the direct binding of GR and MR by immunoprecipitation in COS-1 cells transiently coexpressing CFP–GR and YFP–MR. In transfected COS-1 cells treated with 10^{-6} M CORT, anti-MR antibody coimmunoprecipitated GR from cell extracts, as detected by immunoblotting with anti-GR antibody (Fig. 1*B*, lane 1). Coimmunoprecipitation did not occur in the absence of CORT (Fig. 1*B*, lane 2).

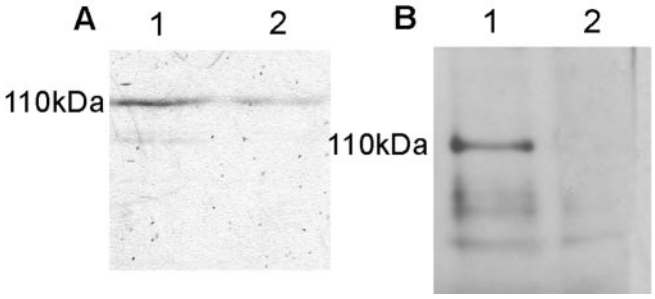

Figure 1. Immunoblotting analysis of fusion proteins and immunoprecipitation. *A*, Immunoblotting of COS-1 cells transfected with CFP–GRNL1$^-$ (lane 1) and wild-type CFP–GR (lane 2) detected with anti-GFP antibody. CFP–GRNL1$^-$- and CFP–GR-transfected cells showed CFP staining at the predicted molecular mass of 110 kDa. *B*, Immunoprecipitation of COS-1 cells transiently expressing CFP–GR and YFP–MR. Anti-MR antibody coimmunoprecipitated GR in cells treated with 10^{-6} M CORT (lane 1) but not in cells that had not been exposed to CORT (lane 2). The arrowhead indicates CFP–GR signal at a molecular mass of 110 kDa.

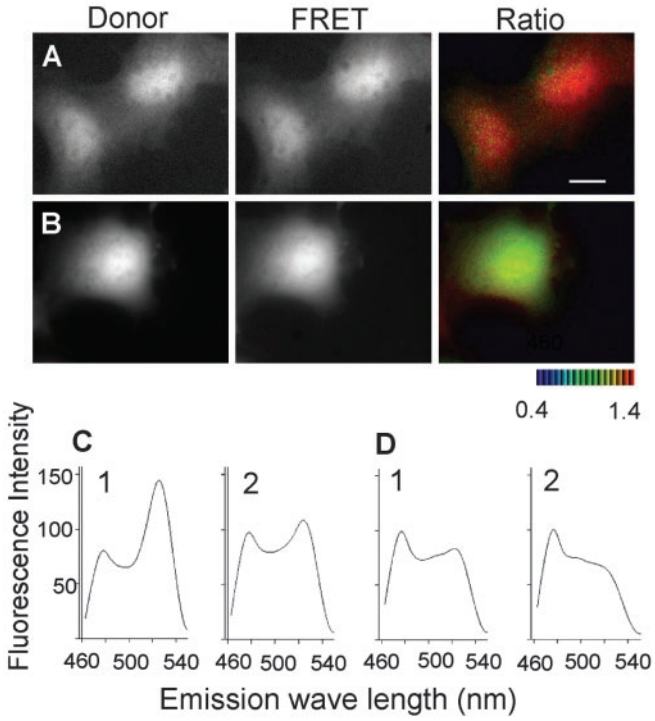

Figure 2. FRET analysis for positive and negative controls. *A*, *B*, Ratio imaging analysis. In each row of images, the ratio image was generated by dividing the FRET by the donor (CFP) fluorescence at each pixel using MetaMorph, as described in Materials and Methods. The hue of each pixel in the ratio image reflects the ratio of that pixel. Scale bar, 10 μm. *A*, COS-1 cells were transfected with a CFP–YFP construct in which CFP and YFP were tandemly linked via three glycine residues. The ratio image showed a red hue, a positive FRET sign, indicating that constitutive FRET occurred. *B*, Negative control. CFP and YFP were independently cotransfected to COS-1 cells. The ratio image showed a green hue, a negative FRET sign. *C*, *D*, Emission-spectral analysis of FRET images in live cells. *C1*, A typical spectrum from a ROI in a COS-1 cell expressing CFP–YFP. Note the prominent peaks at 527 nm. *C2*, After acceptor bleaching at the ROI shown in *C1*, the peak at 527 nm decreased, whereas the peak at 474 nm increased. *D1*, A typical spectrum from an ROI in a COS-1 cell independently expressing CFP and YFP. *D2*, After acceptor bleaching at the ROI shown in *D1*, the peak at 527 nm decreased, whereas the peak at 474 nm did not change.

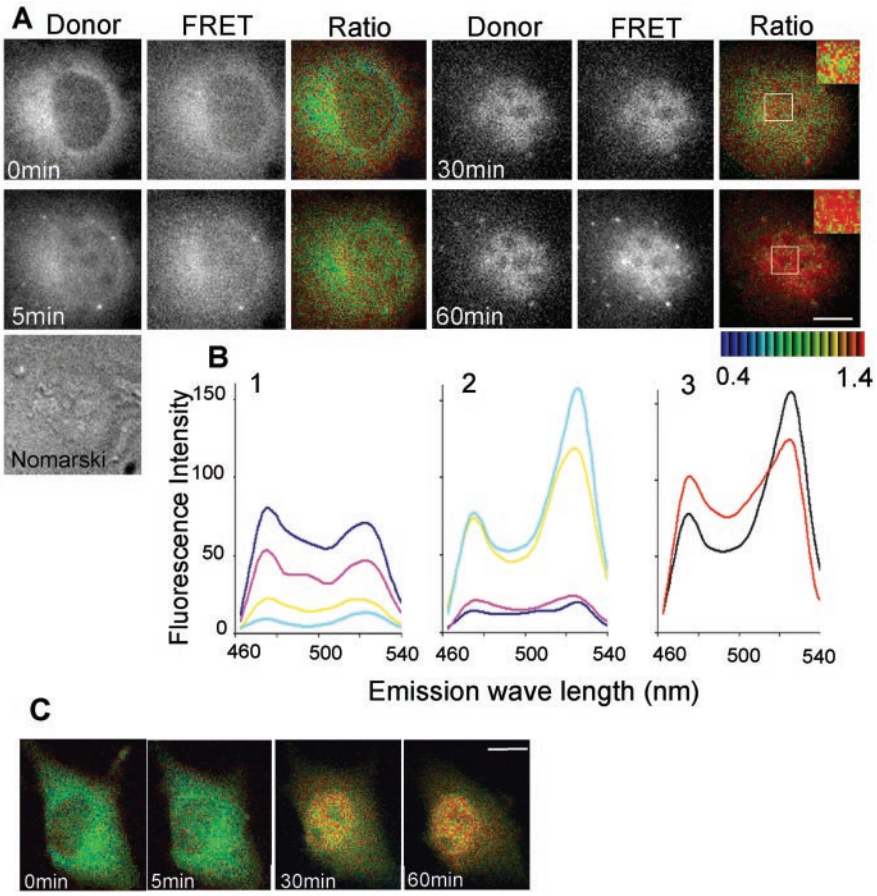

Figure 3. FRET analysis of interactions between CFP–GR and YFP–MR in COS-1 cells. *A*, Ratio imaging analysis. COS-1 cells were cotransfected with CFP–GR and YFP–MR. Images of donor, FRET, and ratio (FRET/donor) were captured at the indicated time after treatment with 10^{-6} M CORT. Areas marked by rectangles in the nucleus of 30 and 60 min are enlarged as insets. Note a red hue showing a positive FRET sign in the nucleus indicated heterodimer formation, whereas very little red hue in the cytoplasm indicated a very low incidence of heterodimerization. The area and intensity of the red hue at 60 min after CORT treatment was more than those at 30 min. Scale bar, 10 μm. *B*, Emission-spectral analysis of FRET images in live cells. *B1*, A typical spectrum from an ROI in the cytoplasm of a COS-1 cell coexpressing CFP–GR and YFP–MR at 0 min (blue), 5 min (pink), 30 min (yellow), and 60 min (cyan) after 10^{-6} M CORT treatment. Note that the peak at 474 nm was a little higher than that at 527 nm, which is similar to the pattern in negative control (see Fig. 2*D1*). The spectral pattern obtained at 5 min after ligand treatment was mostly the same as that observed at 0 min, indicating that FRET did not occur in the cytoplasm. *B2*, A spectrum from ROI in the nucleus of the cell, the spectrum of which is shown in *B1*. Note that the spectral pattern at 30 and 60 min showed the same as those observed in the positive control (see Fig. 2*C1*), indicating that FRET occurred in the nucleus. *B3*, A spectrum before (black) and after (red) acceptor bleaching at 60 min after 10^{-6} M CORT. After acceptor bleaching, the peak at 527 nm decreased, whereas the peak at 474 nm increased, confirming that FRET really occurred. *C*, Ratio imaging analysis with 10^{-9} M CORT. Ratio images of COS-1 cells cotransfected with CFP–GR and YFP–MR at the indicated time after treatment with 10^{-9} M CORT. The red hue was observed in the nucleus at 30 and 60 min after ligand treatment. The degree of red hue was less than that detected with 10^{-6} M CORT. Scale bar, 10 μm.

FRET analysis

Positive and negative control for FRET analysis

We used the GFP-based FRET technique to examine direct GR–MR interactions in living cells. The low level of CFP and YFP bleed-through enabled us to selectively and accurately measure the amounts of CFP–GR and YFP–MR coexpressed in the same cell. Ratio images were presented as pseudocolor, in which the red range indicated a high ratio and the blue range indicated a low ratio. We set up the range of color hue between 1.4 (the highest) and 0.4 (the lowest). As a positive control, the ratio image of COS-1 cells transfected with a CFP–YFP construct, in which CFP and YFP were tandemly linked via three glycine residues, showed a strong red hue in both the cytoplasm and the nucleus, indicating a positive FRET sign (Fig. 2*A*). As a negative control, COS-1 cells cotransfected independently with CFP and YFP showed a green hue in both the cytoplasm and the nucleus, indicating a negative FRET sign (Fig. 2*B*). To semiquantitatively evaluate spectral changes in FRET experiments, we applied a new method of Emission Fingerprinting with LSM 510 META (see Materials and Methods). Figure 2*C1* shows the typical spectral pattern obtained from a ROI in a COS-1 cell expressing CFP–YFP. The mean ratio of fluorescence intensity of 527 and 474 nm (the emission maximum of YFP and CFP, respectively) was 2.06 ± 0.22. We used this spectral pattern as a positive FRET sign in the following FRET analyses. To confirm the occurrence of FRET, we performed acceptor photobleaching, in which energy transfer was detected as an increase in donor (CFP) fluorescence after photobleaching of the acceptor (YFP) (Kinoshita et al., 2001; Mochizuki et al., 2001). YFP was photobleached with 514 nm laser at maximum power for 1 min, and then its spectral image was detected by creating emission spectra. When the same ROI used to create the spectrum shown in Figure 2*C2* were photobleached, the mean reduction in acceptor fluorescence intensity was 27.3 ± 2.2% and the increase in donor fluorescence intensity was 22.5 ± 5.3% (see Fig. 6). In the negative control, in contrast, there was no prominent peak at 527 nm (Fig. 2*D1*), and the mean ratio of fluorescence intensity of 527 and 474 nm was 0.89 ± 0.08. Furthermore, no fluorescence recovery of the donor was detected after acceptor bleaching (Figs. 2*D2*, 6), indicating that FRET did not occur. In both the positive and negative controls, no spectral changes were observed after ligand treatment (data not shown).

FRET analysis in COS-1 cells

Time-lapse ratio images of COS-1 cells coexpressing CFP–GR and YFP–MR revealed that both receptors resided predominantly in the cytoplasm in the absence of ligand, and a green hue diffusely distributed in the cytoplasm indicated a negative FRET sign (Fig. 3*A*,*C*). Although both receptors began nuclear translocation after ligand addition, the ratio image in the cytoplasm at 5 min after treatment with 10^{-6} M CORT still showed mostly green hue, indicating that the receptors did not form heterodimers in the cytoplasm even after ligand binding (Fig. 3*A*). After 30 min, more than half of the receptors resided in the nucleus, and a red hue was detected in the nucleus. After 60 min, however, the density of red hue in the nucleus became higher and a red hue was homogeneously distributed throughout the nucleus, indicating an increase in the amount of heterodimerization of CFP–GR and YFP–MR throughout the entire nucleus (Fig. 3*A*). The brightness of color hue after 60 min was also higher than that after 30 min. Cells cotransfected with CFP–GR and YFP–ERα or with YFP–MR and CFP–ERα did not produce a FRET sign when treated with CORT

(data not shown). Figure 3*B1* shows a typical spectral pattern obtained in the cytoplasm of COS-1 cells coexpressing CFP–GR and YFP–MR at 0, 5, 30, and 60 min after 10^{-6} M CORT. The peak at 474 nm was a little higher than that at 527 nm in the case of 0 and 5 min, as was the case in the negative control shown in Figure 2*D1*. The fluorescence intensity detected at 30 and 60 min in the cytoplasm was very low, because most of the receptors were accumulated in the nucleus at these time points. The mean ratios of fluorescence intensity of 527 and 474 nm detected from the cytoplasm in each time point are shown in Figure 5*A*. Figure 3*B2* shows a typical spectral pattern obtained in the nucleus of COS-1 cells coexpressing CFP–GR and YFP–MR at 0, 5, 30, and 60 min after 10^{-6} M CORT. In contrast to the case of cytoplasm, emission spectra in the nucleus after treatment with 10^{-6} M CORT for 30 and 60 min showed the same pattern as those observed in the positive control in which a prominent peak was detected at 527 nm (Fig. 2*C1*). The mean ratios of fluorescence intensity of 527 and 474 nm detected from the nucleus in each time point are shown in Figure 5*B*. The mean ratio of fluorescence intensity of 527 and 474 nm gradually increased after ligand treatment in the nucleus and reached a maximum level at 60 min. In contrast, the mean ratios in the cytoplasm were not significantly changed after ligand treatment and showed a low level of ~0.8, similar to that of negative control indicating that FRET was not taken place in the cytoplasm. When the same ROI was subjected to acceptor bleaching at 60 min after ligand treatment, the acceptor fluorescence peak at 527 nm decreased by 36 ± 2.4%, whereas the donor fluorescence peak at 474 nm increased by 27 ± 7.6%, confirming that FRET had actually taken place (Figs. 3*B3*, 6).

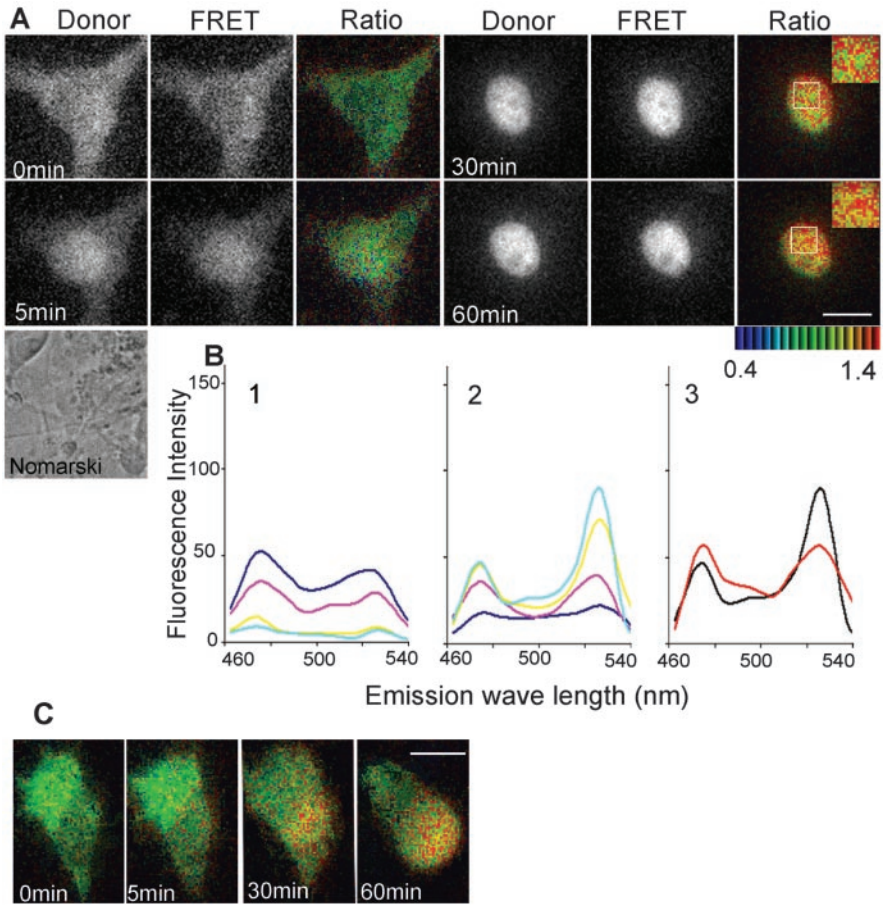

Figure 4. *A*, Ratio imaging analysis. Cultured hippocampal neurons were cotransfected with CFP–GR and YFP–MR. Images of donor, FRET, and ratio (FRET/donor) were captured at the indicated time after treatment with 10^{-6} M CORT. Areas marked by rectangles in the nucleus of 30 and 60 min were enlarged as insets. Note a red hue showing a positive FRET sign in the nucleus indicated heterodimer formation, whereas very little red hue in the cytoplasm indicated a very low incidence of heterodimerization. The area and intensity of the red hue at 60 min after CORT treatment was more than those at 30 min. Scale bar, 10 μm. *B*, Emission-spectral analysis of FRET images in live cells. *B1*, A typical spectrum from ROI in the cytoplasm of a cultured hippocampal neuron coexpressing CFP–GR and YFP–MR at 0 min (blue), 5 min (pink), 30 min (yellow), and 60 min (cyan) after 10^{-6} M CORT treatment. Note that the peak at 474 nm was a little higher than that of 527 nm, which is similar to the pattern in the negative control (see Fig. 2*D1*). The spectral pattern obtained at 5 min after ligand treatment was mostly the same as that observed at 0 min, indicating that FRET did not occur in the cytoplasm. *B2*, A spectrum from ROI in the nucleus of the cell, the spectrum of which was shown in *B1*. Note that the spectral pattern at 30 and 60 min showed the same as those observed in the positive control (Fig. 2*C1*), indicating that FRET occurred in the nucleus. *B3*, A spectrum before (black) and after (red) acceptor bleaching at 60 min after 10^{-6} M CORT. After acceptor bleaching, the peak at 527 nm decreased, whereas the peak at 474 nm increased, confirming that FRET really occurred. *C*, Ratio imaging analysis with 10^{-9} M CORT. Ratio images of cultured hippocampal neurons cotransfected with CFP–GR and YFP–MR at the indicated time after treatment with 10^{-9} M CORT. The red hue was observed in the nucleus at 30 and 60 min after ligand treatment. The degree of the red hue was less than that detected with 10^{-6} M CORT. Scale bar, 10 μm.

To investigate the effects of CORT concentration on heterodimer formation, we treated the cells with a lower concentration of CORT, 10^{-9} M. Under this condition, the density of red hue after ligand treatment was less than the case of 10^{-6} M CORT in ratio image (Fig. 3*C*), and the mean ratios of fluorescence intensity of 527 and 474 nm detected from the nucleus showed lower values than those detected at 10^{-6} M CORT (Fig. 5*B*). Significant difference in the mean ratio between 10^{-6} and 10^{-9} M was obtained after 60 min of CORT treatment. These results indicated that the amount of GR–MR heterodimer was higher at 10^{-6} M CORT than at 10^{-9} M CORT.

FRET analysis in cultured hippocampal neurons

We performed the same experiments in the cultured hippocampal neurons. In the absence of ligand, both receptors resided mainly in the cytoplasm, and a green hue was mostly observed in the ratio image, indicating no heterodimerization (Fig. 4*A*). There was still very few signs of heterodimerization in the cytoplasm at 5 min after treatment with 10^{-6} M CORT. After 30 min, a red hue was detected in the nucleus. The density of the red hue increased at 60 min after CORT treatment. Furthermore, the distribution of red hue in the nucleus was more heterogeneous and located in more restricted regions compared with COS-1 cells (Fig. 4*A*). Figure 4*B1* shows a typical spectral pattern obtained in the cytoplasm of cultured hippocampal neurons coexpressing CFP–GR and YFP–MR at 0, 5, 30, and 60 min after 10^{-6} M CORT. The peak at 474 nm was a little higher than that at 527 nm in the case of 0 and 5 min, as was the case in the negative control shown in Figure 2*D1*. The fluorescent intensity detected

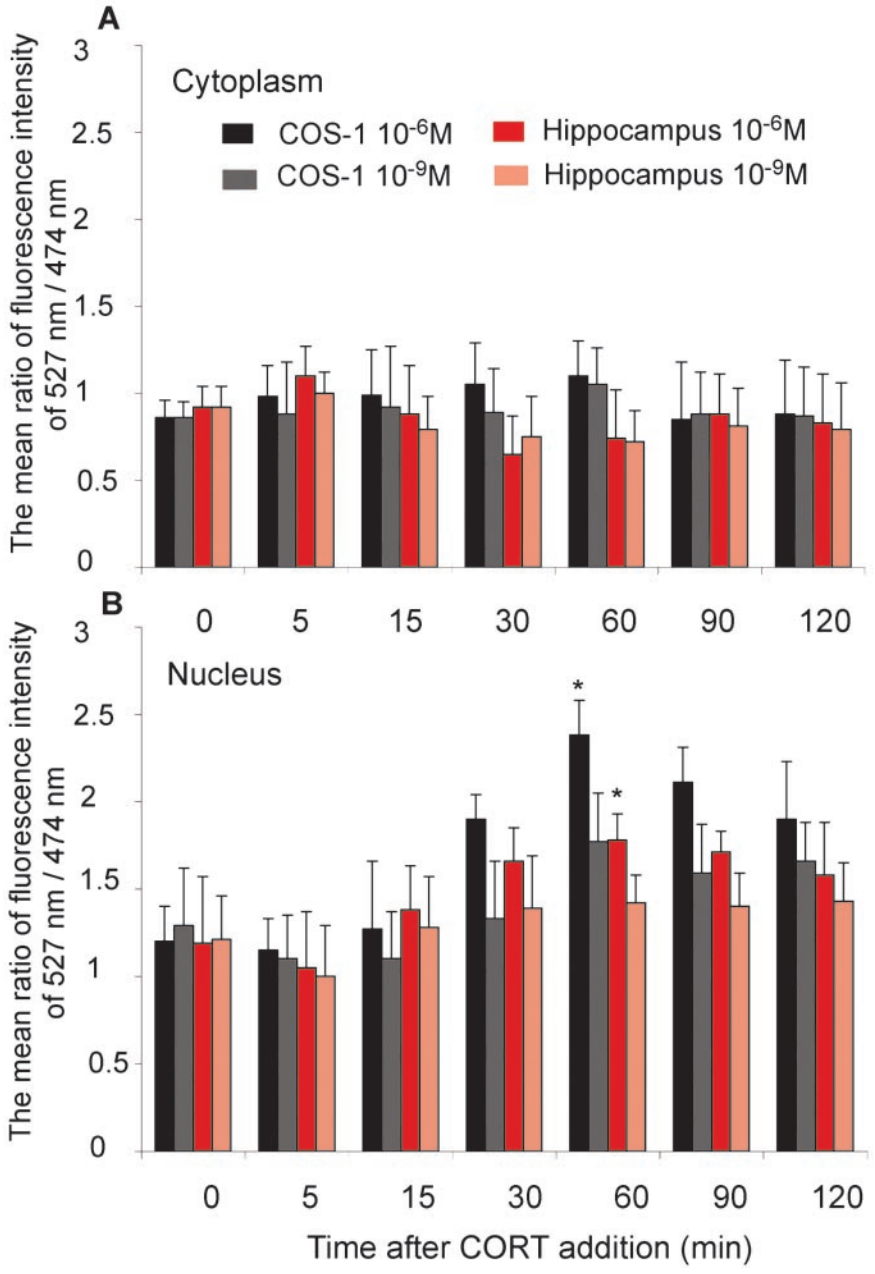

Figure 5. Time course changes in the mean ratio of fluorescence intensity of 527 and 474 nm detected in the cytoplasm (*A*) and in the nucleus (*B*). COS-1 cells and cultured hippocampal neurons coexpressed with CFP–GR and YFP–MR were subjected to Emission Fingerprinting analysis, and spectral changes were detected at the indicated time after treatment with 10^{-6} or 10^{-9} M CORT in both the cytoplasm and the nucleus. Then, the mean ratios of fluorescence intensity of 527 and 474 nm were calculated from 20 ROI per cell in 10 cells of three independent experiments. The mean ratios of fluorescence intensity of 527 and 474 nm in the cytoplasm showed mostly the same values of ~0.8, similar to that of the negative control. In contrast, the mean ratios in the nucleus gradually increased and reached a maximum level after 60 min of CORT treatment. *Significant differences between 10^{-6} and 10^{-9} M CORT were obtained at 60 min after CORT treatment in both COS-1 cells and cultured hippocampal neurons ($p < 0.05$).

at 30 min and 60 min in the cytoplasm was very low, because most of the receptors were accumulated in the nucleus at these time points. The mean ratios of fluorescence intensity of 527 and 474 nm detected from the cytoplasm in each time point were shown in Figure 5*A*. Figure 4*B2* shows a typical spectral pattern obtained in the nucleus of cultured hippocampal neurons coexpressing CFP–GR and YFP–MR at 0, 5, 30, and 60 min after 10^{-6} M CORT. In contrast to the case of cytoplasm, emission spectra in the nucleus after treatment with 10^{-6} M CORT for 30 and 60 min showed the same pattern as those observed in the positive control in which a prominent peak was detected at 527 nm (Fig. 2*C1*). The mean ratios of fluorescence intensity of 527 and 474 nm detected from the nucleus in each time point are shown in Figure 5*B*. The mean ratio of fluorescence intensity of 527 and 474 nm gradually increased after ligand treatment in the nucleus and reached a maximum level at 60 min, whereas the mean ratios in the cytoplasm were not significantly changed after ligand treatment and showed low levels similar to that of the negative control, indicating that FRET did not occur in the cytoplasm. When the same ROI detected at 60 min after ligand treatment was subjected to acceptor bleaching, the acceptor fluorescence peak at 527 nm decreased by 32 ± 2.4%, whereas the donor fluorescence peak at 474 nm increased by 20 ± 6%, verifying that FRET had actually taken place (Figs. 4*B3*, 6). In the case of 10^{-9} M CORT, we detected less red hue (Fig. 4*C*) and lower mean ratio values with spectral analysis (Fig. 5*B*) in the nucleus compared with those detected at 10^{-6} M. A significant difference in the mean ratio between 10^{-6} and 10^{-9} M was obtained after 60 min of CORT treatment. These results indicated that the amount of GR–MR heterodimer in the cultured hippocampal neurons was higher at 10^{-6} M CORT than at 10^{-9} M CORT.

To compensate for different levels of protein expression in different cells, we divided the mean ratio of fluorescence intensity of 527 and 474 nm at the indicated times after ligand addition by the mean ratio of fluorescence intensity of 527 and 474 nm before ligand treatment in each cell. The result, which we call the normalized ratio, reflected more precise changes in fluorescence intensity before and after ligand treatment (Table 1). The normalized ratio at 10^{-6} M CORT is higher than that at 10^{-9} M CORT in both COS-1 cells and cultured hippocampal neurons. Compared with COS-1 cells, the increase in the ratio of cultured hippocampal neurons was smaller at both concentrations of CORT.

Subcellular trafficking analysis with nuclear localization signal mutant

To confirm our observations, we used the mutant CFP–GRNL1$^-$ that lacked nuclear translocation ability. When this construct was singly transfected into COS-1 cells, they resided in the cytoplasm in the absence and the presence of ligand (data not shown). When CFP–GRNL1$^-$ was cotransfected with wild-type YFP–MR, wild-type YFP–MR was completely translocated to the nucleus 60 min after 10^{-6} M CORT treatment, whereas mutated CFP–GRNL1$^-$ showed very little nuclear translocation (Fig. 7*A*). The ratio image of FRET analysis showed that only a very low FRET sign was being

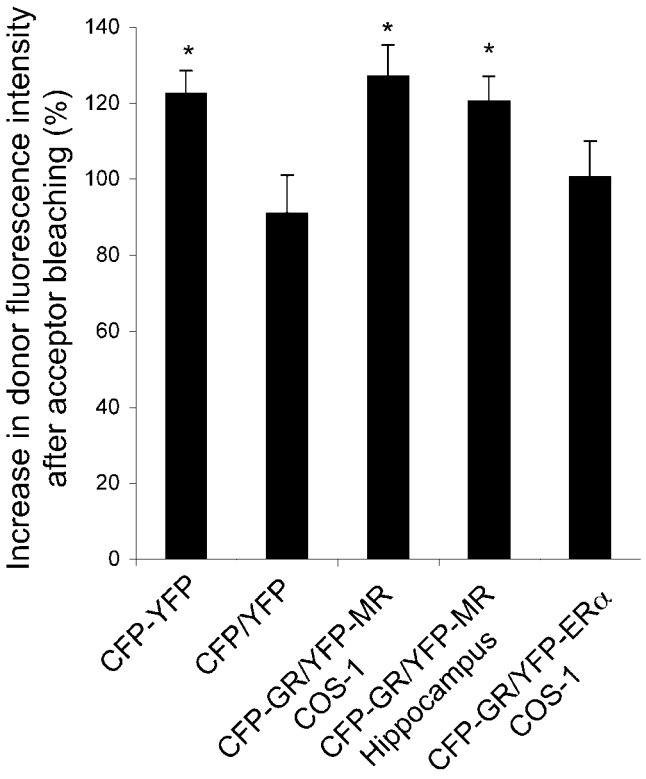

Figure 6. Changes in donor fluorescence intensity after acceptor bleaching. COS-1 cells expressing CFP–YFP (positive control), CFP–YFP (negative control), CFP–GR and YFP—MR, and CFP–GR and YFP–ERα and cultured hippocampal neurons expressing CFP–GR and YFP–MR were subjected to acceptor bleaching as described in Materials and Methods. In the case of CFP–GR and YFP–MR, the cells were treated with 10^{-6} M. Each bar is the mean of 15 cells in three independent experiments. In each ROI, we calculated the change in donor fluorescence dividing the fluorescence intensity after acceptor bleaching by the intensity before acceptor bleaching. *Significantly different from negative control ($p < 0.05$).

Table 1. Ratios for normalization

	CORT treatment			
	10^{-6} M		10^{-9} M	
	COS-1 cells	Hippocampal neurons	COS-1 cells	Hippocampal neurons
5 min	1.13	1.11	1.02	1.01
15 min	1.47	1.46	1.28	1.29
30 min	2.21	1.69	1.55	1.47
60 min	2.76	1.81	2.06	1.57

The ratio for normalization was obtained by dividing the mean ratio of fluorescence intensity of 527 and 474 nm at the indicated times after ligand addition by the mean ratio of fluorescence intensity of 527 and 474 nm before ligand treatment to compensate for different levels of protein expression in different cells.

detected in COS cells coexpressing CFP–GRNL1$^-$ and wild-type YFP–MR at 5 min after treatment with CORT. Because the dimerization domains of mutant construct are intact (Savory et al., 2001), these results suggest that GR and MR do not form heterodimers in the cytoplasm even after ligand treatment.

Discussion

We reported previously that the GR and MR are rapidly translocated from the cytoplasm to the nucleus in neurons and nonneural cells in a ligand-dependent manner (Nishi et al., 1999, 2001). Recently, we also clarified that importin α and β are involved in the nuclear translocation of GR and MR and the spatiotemporal relationships of these molecules in living cells using the FRET technique (Tanaka et al., 2003; M. Tanaka, M. Nishi, M. Kawata, unpublished observations).

In the present study, we focused on the dynamic interaction between the GR and MR in living cells. Heterodimerization between transcription factors is not uncommon and seems to increase the level of functional diversity (Forman and Samuels, 1990; Power et al., 1992). Likewise, the formation of heterodimers between members of the nuclear receptor superfamily is a common property. Interactions have been reported between the retinoic X receptor and the retinoic acid receptor, and between the vitamin D receptor and the thyroid receptor (Kliewer et al., 1992). The same could be true for the case of GR and MR. Previous molecular biological studies have indicated that in cells expressing only one of the receptors, transcriptional regulation from HREs, many of which are imperfect inverted hexanucleotide repeats, is mediated by receptor homodimers (Dahlman et al., 1989; Umesono and Evans, 1989; Forman et al., 1995). However, physiological studies in various systems also suggest that the GR and MR functionally interact with each other (Gomez-Sanchez et al., 1990; Joels and de Kloet, 1992). Biogenetic evidence demonstrated that the GR (Umesono and Evans, 1989) and the MR (Govindan et al., 1991) form homodimers through a dimer interface within their zinc finger regions (ZFRs), and these receptors share complete sequence identity in this ZFR dimer interface, suggesting that this region might mediate heterodimerization as well (Liu et al., 1995). To look for such an interaction in a spatiotemporal-specific manner, we conducted a FRET analysis coupled with a new technique called spectral imaging fluorescence microscopy (Lansford et al., 2001; Hiraoka et al., 2002) to compensate for varying levels of protein expression. This technique allowed us to detect spectral changes in fluorescence in living cells and to address several controversial points of intermolecular FRET (Miyawaki and Tsien, 2000). We calculated the mean ratios of fluorescence intensity of acceptor and donor emission maximum wavelengths, 527 and 474 nm, respectively. We divided the mean ratio of fluorescence intensity of 527 and 474 nm at the indicated times after ligand addition by that detected before ligand treatment. The result, which we call the normalized ratio, reflected more precise changes in fluorescence intensity before and after ligand treatment. By using these methods, we were able to demonstrate that CFP–GR and YFP–MR directly interact with each other in the nucleus but not in the cytoplasm, after treatment with CORT, both in COS-1 cells and cultured hippocampal neurons. The degree of heterodimer formation gradually increased in the nucleus and reached a maximum level after 60 min of CORT treatment in both cell types. These results suggest that heterodimer formation depends on the content of GR and MR in the nucleus, because both receptors are completely accumulated in the nucleus after 60 min. Because there is the possibility that the various functions of the GR and MR may reflect the differences in their affinity for the common ligand, CORT, we then investigated whether GR and MR heterodimer formation is affected by varying concentrations of CORT.

Particularly in structures such as the hippocampus, where both GR and MR are coexpressed in the same cells (van Steensel et al., 1996), heterodimerization of these receptors may have a decisive influence on the regulation of corticosteroid-responsive genes in the brain. We used two different concentrations, 10^{-6} M CORT, which is much higher than physiological concentrations, and 10^{-9} M, which is between the K_d values of the MR and GR. We found that the amount of heterodimer of CFP–GR and YFP–MR detected at 10^{-6} M was higher than that at 10^{-9} M. These results suggest that MR, with a 10-fold higher affinity than GR,

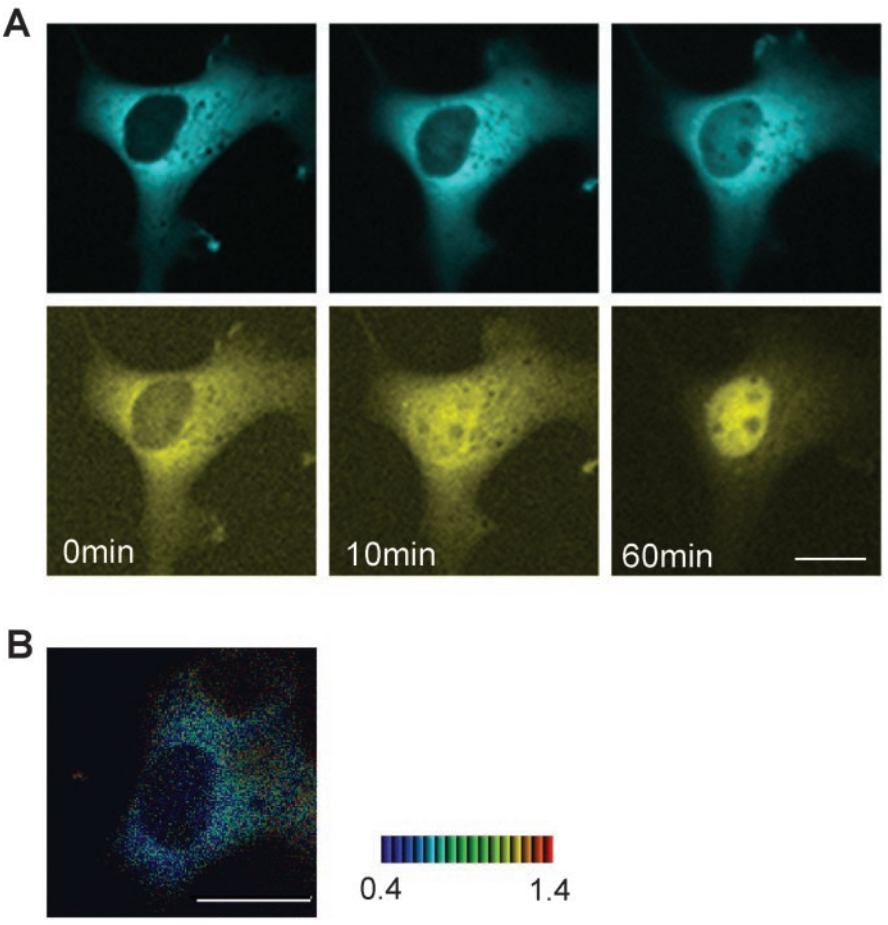

Figure 7. Nuclear trafficking analysis with nuclear translocation mutants. *A*, Time-lapse fluorescence images of COS-1 cells cotransfected with CFP–GRNL1$^-$ and wild-type YFP–MR. In the presence of ligand, the wild-type receptors were translocated into the nucleus, but the mutant receptors were not, indicating the absence of heterodimer formation in the cytoplasm. *B*, Ratio image of FRET analysis in COS-1 cells cotransfected with CFP–GRNL1$^-$ and wild-type YFP–MR 5 min after CORT treatment. A very low FRET sign was observed in the cytoplasm, indicating no heterodimer formation. Scale bar, 10 μm.

may predominantly form homodimers at lower concentrations, whereas at higher concentrations mimicking stressful conditions, the predominance of GR increases to promote the incidence of heterodimerization. Our findings are consistent with the previous demonstrations that MR is predominantly active at lower concentrations to exploit tonic influences, whereas the additional occupancy of GR with higher levels of CORT mediates the feedback actions to restore disturbances of homeostasis (Magarinos et al., 1996; de Kloet et al., 1998). We also observed that GR–MR heterodimers were distributed in more restricted regions of the nucleus in cultured hippocampal neurons than in COS-1 cells. Because endogenous GR and MR are expressed in cultured hippocampal neurons (Bohn et al., 1994), but not in COS-1 cells (Nishi et al., 1999), the heterodimers of GR and MR in cultured hippocampal neurons may present a more physiological distribution pattern, restricting to HREs of targeting genes, than in the case of COS-1 cells.

The results obtained by FRET experiments were supported by trafficking analyses using nuclear translocation mutant of GR, in which the dimerization domains remained intact. Our results suggest that heterodimer formation between the GR and MR is required for corticosteroid-mediated transcription in the nuclear region but not essentially involved in the regulation of nuclear translocation of these receptors. Activated GR or MR may block the activity of other transcription factors, such as activator protein-1 and nuclear factor κB, by direct protein–protein interaction rather than by dimer formation (Ray and Prefontaine, 1994; Guardiola-Diaz et al., 1996; Webster and Cidlowski, 1999). For such interactions to occur, the receptors may have the flexibility to exist as monomers in the nucleus under certain conditions. In contrast to our findings, Savory et al. (2001) reported that the GR and MR formed both heterodimers and homodimers through alternative dimerization interfaces in the cytoplasm. They used myc-tagged GR_{NL1-} mutants, examined receptor redistribution in fixed COS-7 cells, and then detected GR immunoreactivity using an anti-myc antibody. In their experiments, wild-type receptor and mutated receptor constructs were transfected at least 4:1, whereas equal amounts were transfected in the present study. Although the discrepancy between their results and ours may be attributed to the different detection systems and expression conditions of the receptors, the reason for this discrepancy remains unclear.

The physiological significance of the formation of GR–MR heterodimers has been proposed from the colocalization of these receptors in a variety of tissues and cells (Bohn et al., 1994; de Kloet et al., 1998). Hence, having two types of receptors may allow a more flexible response to widely varying corticosteroid concentrations that may be present under physiological and pathological conditions (Trapp and Holsber, 1996). When both GR and MR are expressed in the same cell like hippocampal neurons, their relative concentrations and the ligand concentration will define the proportion of each receptor dimer with its particular DNA-binding and transcriptional activities. The availability of a variety of corticosteroid receptor dimers gives the cell the potential to provide a more finely orchestrated regulation of corticosteroid-responsive genes than the previous model of corticosteroid action based on homodimerization (Evans and Arriza, 1989), although the real functional role of heterodimerization *in vivo* remains controversial. Trapp et al. (1994) indicated that GR and MR activate transcription synergistically through heterodimerization, whereas Liu et al. (1995) reported inhibitory regulation through heterodimerization. A recent study showed the strong expression of 5-HT1A receptors in MR-enriched hippocampal CA1 pyramidal cells and the cooperative interactions between GR and MR at the 5-HT1A-negative glucocorticoid response element (Ou et al., 2001). These findings suggest that the heterodimerization of these receptors is the key mechanism for inhibitory regulation by corticosteroid of the 5-HT1A receptor gene in the brain (Ou et al., 2001). The explanation for this opposite effect and the role of heterodimerization is still ambiguous, and the differences in transfection conditions, cell types, reporters, or promoters must be taken into consideration. Transcriptional cofactors are also another very important player to consider when evaluating the transcription activities of

the GR and MR (Amazit et al., 2003), which were not discussed in the previous studies reporting heterodimer of GR and MR.

In conclusion, FRET analysis clearly demonstrated that GR and MR physically interact with each other in the nucleus of living cultured hippocampal neurons and non-neural cells after CORT treatment. These results indicate that heterodimerization of GR and MR may provide a spatiotemporally specific system for regulating gene expression in response to various cellular environments such as fluctuating CORT concentrations. We demonstrated valuable information that GR and MR form heterodimers in the nucleus after ligand treatment and that this heterodimer formation was more efficient at higher concentrations of CORT, suggesting that GR–MR heterodimers play a more important role under stress conditions. Additional studies will be required to elucidate whether the functional significance of our *in vitro* observations, including the differences between 10^{-6} and 10^{-9} M CORT, also hold true *in vivo*. Understanding the flexible behavior of corticosteroid receptors, particularly in the structures such as hippocampus that are mainly involved in the regulation of stress, mood, learning, and memory, could be useful for the management of stress.

References

Amazit L, Alj Y, Tyagi RK, Chauchereau A, Loosfelt H, Pichon C, Pantel J, Foulon-Guinchard E, Leclerc P, Milgrom E, Guiochon-Mantel A (2003) Subcellular localization and mechanisms of nuclearcytoplasmic trafficking of steroid receptor coactivator-1. J Biol Chem 278:32195–32203.

Arriza JL, Simerly RB, Swanson LW, Evans RM (1988) The neuronal mineralocorticoid receptor as a mediator of glucocorticoid response. Neuron 1:887–900.

Beaumont K, Fanestil DD (1988) Characterization of rat brain aldosterone receptors reveals high affinity for corticosterone. Endocrinology 113:2043–2049.

Bohn MC, O'Banion MK, Young DA, Giuliano R, Hussain S, Dean DO, Cunningham LA (1994) In vitro studies of glucocorticoid effects on neurons and astrocytes. Ann NY Acad Sci 746:243–259.

Dahlman K, Stromatedt PE, Rae C, Jornvall H, Flock JI, Carlstedt-Duke J, Gustafsson JA (1989) High level expression in *Escherichia coli* of the DNA-binding domain of the glucocorticoid receptor in a functional form utilizing domain-specific cleavage of a fusion protein. J Biol Chem 264:804–809.

DeFranco DB (2002) Navigating steroid hormone receptors through the nuclear compartment. Mol Endocrinol 16:1449–1455.

de Kloet ER (1991) Brain corticosteroid receptor balance and homeostatic control. Front Neuroendocrinol 12:95–164.

de Kloet ER, Vreugdenhil E, Oitzl MS, Joels M (1998) Brain corticosteroid receptor balance in health and disease. Endocr Rev 19:269–301.

Evans RM, Arriza JL (1989) A molecular framework for the actions of glucocorticoid hormones in the nervous system. Neuron 2:1105–1112.

Fejes-Toth G, Pearce D, Naray-Fejes-Toth A (1998) Subcellualr localization of mineralocorticoid receptors in living cells: effects of receptor agonists and antagonists. Proc Natl Acad Sci USA 95:2973–2978.

Forman BM, Samuels HH (1990) Interactions among a subfamily of nuclear hormone receptors: the regulatory zipper model. Mol Endocrinol 4:1293–1301.

Forman BM, Umesono K, Chen J, Evans RM (1995) Unique response pathways are established by allosteric interactions among nuclear hormone receptors. Cell 81:541–550.

Funder JW (1996) Mineralocorticoid receptors and glucocorticoid receptors. Clin Endocrinol 45:651–656.

Gomez-Sanchez EP, Venkataraman MT, Thwaites D, Fort C (1990) ICV infusion of corticosterone antagonizes ICV-aldosterone hypertension. Am J Physiol 258:E649–E653.

Gould E, Tanapat P, McEwen BS (1997) Activation of type 2 adrenal steroid receptor can rescue granule cells from death during development. Brain Res Dev Brain Res 101:265–268.

Govindan MV, Leclerc S, Roy R, Rathanaswami P, Xie BX (1991) Differential regulation of mouse mammary tumor virus-bacterial chloramphenicol acetyltransferase chimeric gene by human mineralocorticoid hormone-receptor complexes. J Steroid Biochem Mol Biol 39:91–103.

Guardiola-Diaz HM, Kolinske JS, Gates LH, Seasholtz AF (1996) Negative glucocorticoid regulation of cyclic adenosine 3′,5′-monophosphate-stimulated corticotropin-releasing hormone-reporter expression in AtT-20 cells. Mol Endocrinol 10:317–329.

Hiraoka Y, Shimi T, Haraguchi T (2002) Multispectral imaging fluorescence microscopy for living cells. Cell Struct Funct 27:367–374.

Htun H, Barsony J, Renyi I, Gould D, Hager GL (1996) Visualization of glucocorticoid receptor translocation and intranuclear organization in living cells with a green fluorescent protein chimera. Proc Natl Acad Sci USA 93:4845–4850.

Ito T, Morita N, Nishi M, Kawata M (2000) In vitro and in vivo immunohistochemistry for the distribution of mineralocorticoid receptor with specific antibody. Neurosci Res 37:173–182.

Joels M, de Kloet ER (1992) Coordinative mineralocorticoid and glucocorticoid receptor-mediated control of responses to serotonin in rat hippocampus. Neuroendocrinology 55:344–350.

Joels M, de Kloet ER (1994) Mineralocorticoid and glucocorticoid receptors in the brain. Implication for ion permeability and transmitter systems. Prog Neurobiol 43:1–36.

Kawata M (1995) Roles of steroid hormones and their receptors in structural organization in the nervous system. Neurosci Res 24:1–46.

Kinoshita A, Whelan CM, Smith CJ, Mikhalienco I, Rebeck GW, Strickland DK, Hyman BT (2001) Demonstration by fluorescence resonance energy transfer of two sites of interaction between the low-density lipoprotein receptor-related protein and the amyloid precursor protein: role of the intracellular adapter protein Fe65. J Neurosci 21:8354–8361.

Kliewer SA, Umesono K, Mangelsdorf DJ, Evans RM (1992) Retinoid X receptor interacts with nuclear receptors in retinoic acid, thyroid hormone and vitamin D3 signaling. Nature 355:446–449.

Krozowski ZS, Funder JW (1983) Renal mineralocorticoid receptors and hippocampal corticosterone binding species have identical intrinsic steroid specificity. Proc Natl Acad Sci USA 80:6056–6060.

Lansford R, Bearman G, Fraser SE (2001) Resolution of multiple green fluorescent protein color variants and dyes using two-photon microscopy and imaging spectroscopy. J Biomed Optics 6:311–318.

Liu W, Wang J, Sauter NK, Pearce D (1995) Steroid receptor heterodimerization demonstrated in vitro and in vivo. Proc Natl Acad Sci USA 92:12480–12484.

Magarinos AM, McEwen BS, Flugge G, Fuchs E (1996) Chronic psychosocial stress causes apical dendritic atrophy of hippocampal CA3 pyramidal neurons in subordinate tree shrews. J Neurosci 16:3534–3540.

Matsuda K, Ochiai I, Nishi M, Kawata M (2002) Colocalization and ligand-dependent discrete distribution of the estrogen receptor (ER)α and ERβ. Mol Endocrinol 16:2215–2230.

McEwen BS (1991) Non-genomic and genomic effects of steroids on neural activity. Trends Pharmacol Sci 12:141–147.

McEwen BS, de Kloet ER, Rostene W (1986) Adrenal steroid receptors and actions in the nervous system. Physiol Rev 66:1121–1187.

McNally JG, Muller WG, Walker D, Wolford R, Hager GL (2000) The glucocorticoid receptor: rapid exchange with regulatory sites in the living cells. Science 287:1262–1265.

Miyawaki A, Tsien RY (2000) Monitoring protein conformations and interactions by fluorescence resonance energy transfer between mutants of green fluorescent protein. Methods Enzymol 327:472–500.

Mochizuki N, Yamashita S, Kurokawa K, Ohta Y, Nagai T, Miyawaki A, Matsuda M (2001) Spatio-temporal images of growth-factor-induced activation of Ras and Rap1. Nature 411:1065–1068.

Morimoto M, Morita N, Ozawa H, Yokoyama K, Kawata M (1996) Distribution of glucocorticoid receptor immunoreactivity and mRNA in the rat brain: an immunocytochemical and in situ hybridization study. Neurosci Res 26:235–269.

Nishi M, Takenaka N, Morita N, Ito T, Ozawa H, Kawata M (1999) Real-time imaging of glucocorticoid receptor dynamics in living neurons and glial cells in comparison with non-neural cells. Eur J Neurosci 11:1927–1936.

Nishi M, Ogawa H, Ito T, Matsuda K, Kawata M (2001) Dynamic changes in subcellular localization of mineralocorticoid receptor in living cells: in comparison with glucocorticoid receptor using dual-color labeling with green fluorescent protein spectral variants. Mol Endocrinol 15:1077–1092.

Ou XM, Storring JM, Kushwaha N, Albert PR (2001) Heterodimerization of

mineralocorticoid and glucocorticoid receptors at a novel negative response element of the 5-HT1A receptor gene. J Biol Chem 276:14299–14307.

Pearce D, Yamamoto KR (1993) Mineralocorticoid and glucocorticoid receptor activities distinguished by nonreceptor factors at a composite response element. Science 259:1161–1165.

Power RF, Conneely OM, O'Malley BW (1992) New insights into activation of the steroid hormone receptor superfamily. Trends Pharmacol Sci 13:318–323.

Ray A, Prefontaine KE (1994) Physical association and functional antagonism between the p65 subunit of transcriptional factor NF-κB and the glucocorticoid receptor. Proc Natl Acad Sci USA 91:752–756.

Reits EAJ, Neefjes JJ (2001) From fixed to GRAP: measuring protein mobility and activity in living cells. Nat Cell Biol 3:E145–E147.

Reul JMHM, de Kloet ER (1985) Two receptor systems for corticosterone in rat brain: microdistribution and differential occupation. Endocrinology 117:2505–2511.

Rupprecht R, Reul JMHM, van Steensel B, Spengler D, Soder M, Berning B, Holsboer F, Damm K (1993) Pharmacological and functional characterization of human mineralocorticoid and glucocorticoid receptor ligands. Eur J Pharmacol 247:145–154.

Savory JGA, Hsu B, Laquian IR, Giffin W, Reich T, Hache RJG, Lefebvre YA (1999) Discrimination between NL1$^-$ and NL2$^-$ mediated nuclear localization of the glucocorticoid receptor. Mol Cell Biol 19:1025–1037.

Savory JGA, Prefontaine GG, Lamprecht C, Liao M, Walther RF, Lefebvre YA, Hache RJG (2001) Glucocorticoid receptor homodimers and glucocorticoid-mineralocorticoid receptor heterodimers form in the cytoplasm through alternative dimerization interfaces. Mol Cell Biol 21:781–793.

Stenoien DL, Patel K, Mancini MG, Dutertre M, Smith CL, O'Malley BW, Mancini MA (2001) FRAP reveals that mobility of oestrogen receptor-α is ligand- and proteasome-dependent. Nat Cell Biol 3:15–23.

Tanaka M, Nishi M, Morimoto M, Kawata M (2003) Nuclear import of glucocorticoid receptor in association with importin α and importin β: analysis with real-time fluorescence imaging and fluorescence resonance energy transfer in living cells. Endocrinology 144:4070–4079.

Trapp T, Holsber F (1996) Heterodimerization between mineralocorticoid and glucocorticoid receptors increases the functional diversity of corticosteroid action. Trends Pharmacol Sci 17:145–149.

Trapp T, Rupprecht R, Castren M, Reul JMHM, Holsber F (1994) Heterodimerization between mineralocorticoid and glucocorticoid receptor: a new principle of glucocorticoid action in the CNS. Neuron 13:1457–1462.

Umesono K, Evans RM (1989) Determination of target gene specificity for steroid/thyroid hormone receptors. Cell 57:1139–1146.

van Steensel B, van Binnendijk EP, Hornsby C, van der Voort TM, Krozowski ZS, de Kloet ER, van Driel R (1996) Partial colocalization of glucocorticoid and mineralocorticoid receptors in discrete compartments in nuclei of rat hippocampal neurons. J Cell Sci 109:787–792.

Webster JC, Cidlowski JA (1999) Mechanisms of glucocorticoid-receptor-mediated repression of gene expression. Trends Endocrinol Metab 10:396–402.